Interannual variation in solar heating in the Chukchi Sea, Arctic Ocean

Yushiro Tsukada[1]・Hiromichi Ueno[1]・Naoki Ohta[2]・Motoyo Itoh[3]・Eiji Watanabe[3]・Takashi Kikuchi[3]・Shigeto Nishino[3]・Kohei Mizobata[4]

1 Graduate School of Fisheries Sciences, Hokkaido University, 3-1-1 Minato-cho, Hakodate, 041-8611 Japan

2 Graduate School of Environmental Science, Hokkaido University, N10 W5 Kita-ku, Sapporo, 060-0810 Japan.

3 Institute of Arctic Climate and Environment Research, Japan Agency for Marine-Earth Science and Technology, 2-15 Natsushima-cho, Yokosuka 237-0061, Japan

4 Department of Ocean Sciences, Tokyo University of Marine Science and Technology, 4-5-7 Konan, Minato-ku, Tokyo 108-8477, Japan

Author for correspondence: Hiromichi Ueno, Faculty of Fisheries Sciences, Hokkaido University, 3-1-1 Minato-cho, Hakodate, 041-8611 Japan. Email: ueno@fish.hokudai.ac.jp

Keywords

Solar heating; Chukchi Sea; Interannual variation

Abstract

Solar heating in summer in the Chukchi Sea was estimated using satellite-derived sea-ice concentration data and reanalysis shortwave radiation data. The shortwave radiation was validated by *in-situ* data obtained by the R/V Mirai and NCEP-CFSR/CFSv2 was found to reproduce *in-situ* data accurately compared with NCEP/NCAR Reanalysis 1 and ERA-Interim. Solar heating integrated over the Chukchi Sea in summer varied interannually from 3.6×10^{20} J in 2000 to 6.7×10^{20} J in 2015, and was up to twice the northward heat flux through the Bering Strait. The total heating in the Chukchi Sea implies that the heat in the Chukchi Sea provided by northward heat flux through the Bering Strait is amplified by solar heating in the Chukchi Sea. We further compared these heat fluxes into the Chukchi Sea with the summertime northward heat flux through Barrow Canyon, an indicator of heat flux from the Chukchi Sea to the Arctic basin. The northward heat flux through Barrow Canyon was affected by the interannual variation of solar heating in the eastern Chukchi Sea. These results imply that modification of Pacific water in the Chukchi Sea by solar heating plays an important role in the interannual variation in heat transport from the Chukchi Sea to the western Arctic basin.

1. Introduction

Summer Arctic sea-ice cover has declined rapidly over the past few decades. The albedo of sea ice is much higher than that of open water; a decrease in sea-ice cover is associated with an increase in solar heating and thus surface warming of the Arctic Ocean (Perovich et al., 2007; Steele et al., 2008). The reduction in sea-ice cover also plays a significant role in the polar

amplification of climate change (Holland and Bitz, 2003; Serreze et al., 2009) and in marine and terrestrial ecological dynamics in the Arctic region (Post et al., 2013).

The largest decline in sea ice occurred in the Pacific region of the Arctic Ocean (Comiso, 2012). Heat transport of Pacific water through the Bering Strait, which has increased in recent years (Woodgate et al., 2006; 2010; 2015), plays an important role in decreasing sea-ice formation during the winter and in sea-ice melt in summer in the Canada basin (Steele et al., 2004; Shimada et al., 2006). In 2007, which was marked by an extreme retreat of Arctic sea ice, the heat transport was sufficient to cause one third of the seasonal Arctic sea-ice loss (Woodgate et al., 2010).

The Chukchi Sea (Fig. 1) is located between the Bering Sea and the Arctic basin and is a pathway for Pacific water from the Bering Strait. We anticipate that solar heating significantly modifies Pacific water in the Chukchi Sea. However, there have been no quantitative analyses of solar heating in the Chukchi Sea except for a rough estimate of 4×10^{20} J yr^{-1} (Woodgate et al., 2010) based on an annual solar heating of ~1,300 MJ m^{-2} yr^{-1} (Perovich et al., 2007) and a Chukchi Sea area of ~350×10^3 km^2. It was also indicated that the annual northward heat flux through the Bering Strait was somewhat greater than annual solar heating in the Chukchi Sea and the former interannual variation was slightly larger than the latter (Woodgate et al., 2010). In this study, we estimated interannual variation in solar heating in summer in the Chukchi Sea by analyzing satellite-derived sea-ice concentration data and reanalysis shortwave radiation data, and compared its impact on the heat budget of the Chukchi Sea with that of heat transport through the Bering Strait after validating the reanalysis data using *in-situ* shortwave radiation data obtained by the R/V Mirai.

2. Data and Methods

The study area was the Chukchi Sea, comprising the shelf area between the Bering Strait and the western Arctic basin (65.45°–75°N, 155°–180°W, excluding the area where water depth was > 200 m, i.e., the area enclosed by the solid black line in Fig. 1). The analysis period was 1999–2015, based on the data available on heat flux through the Bering Strait (Woodgate et al., 2015) and *in-situ* shortwave radiation, as described below. The solar heating (flux of solar heat input to the ocean, F_{rw}) was calculated as follows:

$$F_{rw} = F_r(1-\alpha)(1-C) \quad [\mathrm{W\ m^{-2}}] \qquad (1)$$

according to Perovich et al. (2007). In eq. (1), F_r is downward shortwave radiation, α is the ocean albedo, and C is the sea-ice concentration. We used a value of 0.07 (Pegau and Paulson, 2001) for ocean albedo (α). We considered only the downward solar energy incident on the open ocean, and neglected the downward solar energy incident on/passing through the sea ice, as in Perovich et al. (2007). Recently, it is indicated that light transmission through sea-ice is important for the near-surface temperature maximum structure in Canada Basin (Jackson et al., 2010) and massive phytoplankton blooms under sea-ice in the northern Chukchi Sea (Arrigo et al., 2012). In the Chukchi Sea, it was reported that annual total solar heating through sea-ice ranges from 0.1×10^8 $\mathrm{Jm^{-2}}$ near the Bering Strait to 1×10^8 $\mathrm{Jm^{-2}}$ in the northern Chukchi Sea (Arndt and Nicolaus, 2014). Since sea-ice concentration in the Chukchi Sea is low in summer especially in the southern part, solar heating through sea-ice was much smaller than cumulative solar heating into open ocean from May to September ($3–17 \times 10^8$ $\mathrm{Jm^{-2}}$, see Fig. 5). Therefore, we neglected light transmission through sea-ice in the present study.

For sea-ice concentration (C), we used daily mean 25 km × 25 km data generated from satellite passive microwave observations using the NOAA/NSIDC Climate Data Record (Peng et al., 2013, https://climatedataguide.ucar.edu/climate-data/sea-ice-concentration-noaansidc-climate-data-record). For downward shortwave radiation (F_r), we used data from the following reanalysis products: (1) NCEP/NCAR Reanalysis 1 (Kalnay et al., 1996, http://www.esrl.noaa.gov/psd/data/gridded/data.ncep.reanalysis.tropopause.html, approximately 2°× 2°, daily), (2) ERA-Interim (Dee et al., 2011, http://www.ecmwf.int, 0.125° × 0.125°, 12-hourly) and (3) NCEP-CFSR/CFSv2 (NCEP-CFSR; hereafter, Saha et al., 2010, http://rda.ucar.edu/pub/cfsr.html, about 0.3° × 0.3° for CFSR (1999–2010), approximately 0.2° × 0.2° for CFSv2 (2011–2015), 6-hourly). We evaluated daily solar heating in the grids of the reanalysis products by linearly interpolating sea-ice concentration data to the grid of the reanalysis product. In the present study, we combined satellite sea-ice concentration data with reanalysis downward shortwave radiation data to estimate solar heating; we did not use net surface shortwave radiation data from reanalysis products. This is because (1) satellite sea-ice concentration data were more accurate than those from reanalysis products and (2) we intended to directly validate reanalysis downward shortwave radiation data with *in-situ* data as described below.

Downward shortwave radiation data differ according to the reanalysis product, particularly at high latitudes, due to the scarcity of *in-situ* observations. In this study, we used *in-situ* downward shortwave radiation data obtained by the R/V Mirai (R/V Mirai cruises MR99 [September 1999], MR02 [August–October 2002], MR04 [September–October 2004], MR06 [August–September 2006], MR08 [August–October 2008], MR09 [September–October 2009],

and MR10 [September–October 2010]; http://www.godac.jamstec.go.jp/darwin/e) to validate reanalysis shortwave radiation data in the Chukchi Sea, selecting the most suitable reanalysis data set for our study. We first calculated the 24-h averaged *in-situ* downward shortwave radiation and ship positions (red dots in Fig. 1) from original Mirai data obtained every 10 min. Then, the downward shortwave radiation from the reanalysis products was also 24-h averaged, and linearly interpolated to the positions of the R/V Mirai data. Finally, the two values for the same day and location were compared (176 pairs in total). The *in-situ* data from the R/V Mirai north of the Chukchi Sea were also used because of the scarcity of *in-situ* data within the Chukchi Sea itself.

We used data from the A3 mooring (66.33°N, 168.96°W, 56 m depth) ~60 km north of the Bering Strait (Woodgate et al., 2015, http://psc.apl.washington.edu/HLD/Bstrait/Data/BeringStraitMooringDataArchive.html) during 1999–2015 to evaluate daily ocean heat transport through the Bering Strait, following Woodgate et al. (2012). The daily heat fluxes through Barrow Canyon during 1999–2014 (Itoh et al., 2013) were also used for comparison with the solar heating. For the latent heat, sensible heat and longwave radiation fluxes, we used the reanalysis data used to estimate solar heating (NCEP-CFSR, see next section). The sea-ice melting heat was calculated from the difference in the daily mean sea-ice concentration averaged over the Chukchi Sea between a given day and the previous day, assuming that the sea-ice thickness was 1 m and neglecting sea-ice advection. The value of 1 m is consistent with the average sea-ice thickness of 1.38 m previously observed in the coastal northeastern Chukchi Sea (Fukamachi et al., 2017) and a value of ~ 1.5 m that we derived for the Chukchi Sea during March–April using CryoSat-2 data (http://www.cpom.ucl.ac.uk/csopr/seaice.html). Our analysis was limited to the summer season (May–September), neglecting the heat release due to sea-ice

formation, because sea-ice concentration generally decreases from May to August and starts to increase again in October, and heat transport through the Bering Strait is almost zero before May (Fig. 2). In the present paper, integrated values in summer season for the solar heating, heat fluxes and heat transports (with the unit of J) are discussed.

3 Validation of downward shortwave radiation from reanalysis products

The downward shortwave radiation from the reanalysis products was compared with *in-situ* data obtained by the R/V Mirai. Figure 3 shows day-to-day variation of downward shortwave radiation from reanalysis products and *in-situ* observations. This figure indicates that the values from the reanalysis products mostly follows day-to-day variation of *in-situ* data. The values from the reanalysis products also reproduce decreasing trend of *in-situ* data during each observation period. However, the averaged downward shortwave radiation using all values in Fig. 3 was 41.0, 41.3, 71.8 and 19.8 W m^{-2} for *in-situ* observations, NCEP-CFSR, ERA Interim and NCEP-NCAR Reanalysis 1, respectively: the averaged values from ERA Interim and NCEP-NCAR Reanalysis 1 were smaller and larger than that from *in-situ* data, respectively.

The values from the reanalysis products were all significantly correlated with the *in-situ* values (at the 99% confidence level, Table 1 and Fig. 4). Figure 4 also shows that the values from ERA Interim and NCEP-NCAR Reanalysis 1 were systematically smaller and larger than *in-situ* values, respectively, whereas the values from NCEP-CFSR accurately reproduced *in-situ* data. In addition, the standard deviations of the absolute values of the difference between *in-situ* and reanalysis values were relatively large for ERA Interim and NCEP-NCAR Reanalysis 1 compared with NCEP-CFSR data (Table 1). This finding is consistent with previous studies;

e.g., Lindsay et al. (2014) reported that NCEP-CFSR downward shortwave radiation accurately represented observation data in the Arctic region using two coastal land stations. Therefore, we used NCEP-CFSR downward shortwave radiation data for the analyses below. Although NCEP-CFSR downward shortwave radiation data are concluded to be the most suitable for our analysis based on the comparison with *in-situ* data discussed above, it is important to note that more *in-situ* observations and comparison would be necessary to validate the reanalysis data from the view point of interannual variation. We used the latent heat, sensible heat and longwave radiation flux data from NCEP-CFSR to examine the heat budget in the Chukchi Sea although it is also important to note that good reproduction of shortwave radiation does not always indicate the good reproduction of other components.

4 Interannual variation in solar heating in the Chukchi Sea

Figure 5 shows the horizontal distribution of cumulative solar heating from May to September in the Chukchi Sea, averaged over 1999–2015 and estimated using NCEP-CFSR downward shortwave radiation data. Solar heating generally decreased with latitude because of early sea-ice retreat and late freezing in the southern region. Strong solar heating was also observed along the Alaskan coast probably due to warm Alaskan coastal current. Solar heating integrated over the Chukchi Sea in summer (from May to September) varied interannually from 3.6×10^{20} J in 2000 to 6.7×10^{20} J in 2015 (red line in Fig. 6a). This variation was negatively correlated with sea-ice concentration averaged over the Chukchi Sea in summer (blue line in Fig. 6b; correlation coefficient = -0.91, significant at the 99% confidence level), as expected from eq. (1). In contrast, the downward shortwave radiation averaged over the Chukchi Sea in summer was

less variable compared with solar heating, ranging from 171 W m^{-2} in 2011 to 186 W m^{-2} in 2002 (red line in Fig. 6b), and the correlation coefficient with solar heating was low (-0.25). These results imply that interannual variation in solar heating is influenced by the seasonal timing of open water formation, which is consistent with the result by Steele and Dickinson (2016) that sea surface temperature maximum is correlated with the date of sea-ice retreat in the Pacific Sector of the Arctic Ocean although the correlation coefficient is relatively low in the Chukchi Sea.

The summertime solar heating was considerably (1.3- to 1.9-fold) larger than the northward heat flux through the Bering Strait (purple line in Fig. 6a), ranging from 2.4 $\times 10^{20}$ J in 2012 to 4.7 $\times 10^{20}$ J in 2007. The sea-ice melting heat and the sum of the latent heat, sensible heat and longwave radiation fluxes (all of the radiative heat fluxes except for downward shortwave radiation) were less variable throughout the analysis period, ranging from -2.2 $\times 10^{20}$ J in 2006 to -1.7 $\times 10^{20}$ J in 2011, and -1.5 $\times 10^{20}$ J in 2012 to -0.85 $\times 10^{20}$ J in 2003, respectively (Fig. 6a). The sea-ice melting heat hardly changes inter-annually because sea-ice usually melts completely in the Chukchi Sea every summer. The summertime total heating in the Chukchi Sea (black line in Fig. 6a) was calculated as the sum of solar heating (red line), northward heat flux through the Bering Strait (purple line), sea-ice melting heat (blue line) and sum of the latent heat, sensible heat and longwave radiation fluxes (green line). The heat transport due to water exchange between the Chukchi Sea and Arctic basin, and between the Chukchi and the East Siberian Seas, was not considered in this analysis.

The total heating was positive throughout the analysis period, ranging from 2.9 $\times$ 10^{20} J in 2000 to 8.4 $\times$ 10^{20} J in 2007 (Fig. 6a). The interannual variation in total heating correlated with the interannual variation in the solar heating (correlation coefficient = 0.94; significant at the 99%

confidence level) and the northward heat flux through the Bering Strait (correlation coefficient = 0.89; significant at the 99% confidence level). In addition, the interannual variability in the total heating in the Chukchi Sea (standard deviation = 1.6×10^{20} J) was roughly twice that of the northward heat flux through the Bering Strait (standard deviation = 0.65×10^{20} J) and the solar heating (standard deviation: 0.89×10^{20} J). These results imply that the heat in the Chukchi Sea provided by the northward heat flux through the Bering Strait is amplified by solar heating in the Chukchi Sea.

It is important to note that these results were not sensitive to sea-ice thickness and ocean albedo, which we assumed in our analysis to be as follows: the correlation coefficients between the interannual variation in total heating and northward heat flux through the Bering Strait were 0.91(0.85) for a sea-ice thickness = 0.5(2) m, and 0.89(0.89) for an ocean albedo = 0.0(0.1), respectively. The standard deviation of the interannual variability in total heating was roughly twice that of the northward heat flux through the Bering Strait using these values of sea-ice thickness and ocean albedo.

It was assumed that the total heating in the Chukchi Sea increased the heat content of the water in the Chukchi Sea or was transported to the Arctic basin. However, it was difficult to separate the two heat fluxes or to clarify how the solar heating in the Chukchi Sea influenced heat transport to the Arctic basin. Therefore, we used the summertime northward heat flux through Barrow Canyon (Fig. 6b), one of the major heat transport fluxes from the Chukchi Sea to the Arctic basin (Itoh et al., 2013; Watanabe et al., 2017), to investigate the influence of solar heating in more detail. The summertime mean Pacific water transport through Barrow Canyon represents more than 80% of the long-term mean Pacific water inflow through the Bering Strait (Itoh et al., 2013). The northward annual heat transport through the Barrow Canyon ranges from

0.16×10^{20} J in 2006 to 0.86×10^{20} J in 2003. This value was smaller than the total heating in the Chukchi Sea, probably because the total heating is mostly used to heat the water in the Chukchi Sea.

Comparison between Fig. 6a and 6c shows that the interannual variation in the northward heat flux through Barrow Canyon did not correlate with that through the Bering Strait (correlation coefficient = 0.16), implying that the northward heat flux through the Bering Strait does not control the interannual variation in the northward heat flux through Barrow Canyon. However, the correlation coefficient between the northward heat flux through Barrow Canyon and the solar heating in the Chukchi Sea was 0.65, significant at 95% confidence level. This implies that the solar heating in the Chukchi Sea has a significant impact on the interannual variation in heat transport from the Chukchi Sea to the Arctic basin. While the northward heat flux through Barrow Canyon did not correlate with that through the Bering Strait, the former correlated with the solar heating in the Chukchi Sea, because the residence time for the water in the Chukchi Sea is longer than several months (e.g. Watanabe, 2011).

The correlation coefficients between the northward heat flux through Barrow Canyon and the solar heating distributed from the Bering Strait to the Barrow Canyon were high (> 0.5) in the eastern Chukchi Sea (Fig. 7). This area corresponds to one of three flow paths from the Bering Strait to the Arctic basin (Alaskan Coastal Current; e.g., Weingartner et al., 2005), implying that solar heating along the Alaskan Coastal Current from the Bering Strait to the Barrow Canyon has a significant impact on the interannual variation in the northward heat flux through Barrow Canyon. The area where the correlation coefficient > 0.5 also extended to the west/west-northwest from the canyon. This pattern of distribution of the correlation coefficient might correspond to the flow path from the area around the Hanna Shoal to Barrow Canyon in

Gong and Pickart (2015), who reported that this flow originated from the other flow paths from the Bering Strait: through the Hope Valley into Herald Canyon (Weingartner et al., 1998), and through the Central Channel between the Herald and Hanna Shoals (Weingartner et al., 2005). These results imply that modification of Pacific water by solar heating in the Chukchi Sea plays an important role in interannual variation in heat transport from the Chukchi Sea to the Arctic basin. A more recent study indicates the existence of a westward current from the Barrow Canyon (Chukchi slope current, Corlett and Pickart, 2017); therefore, interannual variation of northward heat flux through Barrow Canyon might further propagate westward along the continental slope.

5. Summary

We estimated interannual variation in solar heating in the Chukchi Sea via analysis of satellite-derived sea-ice concentration data and shortwave radiation reanalysis data. The downward shortwave radiation from the reanalysis products was compared with *in-situ* data obtained by the R/V Mirai. We concluded that NCEP-CFSR data reproduced *in-situ* data most accurately, and used NCEP-CFSR downward shortwave radiation data in our analyses.

Summertime solar heating integrated over the Chukchi Sea varied interannually from 3.6×10^{20} J in 2000 to 6.7×10^{20} J in 2015. The previous estimate of 4×10^{20} J (Woodgate et al., 2010) was included in this range but was on the low end of the variability. The summertime solar heating was negatively correlated with summertime sea-ice concentration averaged over the

Chukchi Sea and was considerably (1.3- to 1.9-fold) larger than the northward heat flux through the Bering Strait. The summertime total heating in the Chukchi Sea, calculated as the sum of solar heating, northward heat flux through the Bering Strait, sea-ice melting heat, and latent heat, sensible heat and longwave radiation fluxes, was positive throughout the analysis period, ranging from 2.9×10^{20} J in 2000 to 8.4×10^{20} J in 2007. The interannual variation in total heating was significantly correlated with the interannual variation in solar heating, as well as with the northward heat flux through the Bering Strait. In addition, the interannual variability in the total heating in the Chukchi Sea was roughly twice that of the northward heat flux through the Bering Strait and the solar heating. These results imply that the heat in the Chukchi Sea provided by the northward heat flux through the Bering Strait is amplified by solar heating in the Chukchi Sea.

We used the summertime northward heat flux through Barrow Canyon, one of the major heat fluxes from the Chukchi Sea to the Arctic basin, to investigate the influence of solar heating in more detail. The interannual variation in the northward heat flux through Barrow Canyon was not correlated with that though the Bering Strait. In contrast, the northward heat flux through Barrow Canyon was significantly correlated with solar heating in the Chukchi Sea, especially along the flow paths from the Bering Strait to Barrow Canyon. This implies that modification of Pacific water in the Chukchi Sea by solar heating plays an important role in heat transport from the Chukchi Sea to the Arctic basin.

Acknowledgement

This study was supported by the Green Network of Excellence (GRENE) Arctic Climate Change Research Project and Arctic Challenge for Sustainability (ArCS) Project, which were founded by the Ministry of Education, Culture, Sports, Science and Technology of Japan (MEXT). The authors thank two anonymous reviewers for their helpful and constructive comments.

References

Arrigo, K. R., Perovich, D. K., Pickart, R. S., Brown, Z. W., van Dijken, G. L., Lowry, K. E., Mills, M. M., Palmer, M. A., Balch, W. M., Bahr, F., Bates, N. R., Benitez-Nelson, C., Bowler, B., Brownlee, E., Ehn, J. K., Frey, K. E., Garley, R., Laney, S. R., Lubelczyk, L., Mathis, J., Matsuoka, A., Mitchell, B. G., Moore, G. W. K., Ortega-Retuerta, E., Pal, S., Polashenski, C. M., Reynolds, R. A., Schieber, B., Sosik, H. M., Stephens, M., and Swift, J. H., 2012. Massive Phytoplankton Blooms Under Arctic Sea Ice, Science, 336, 1408–1408, doi:10.1126/Science.1215065.

Arndt, S. and Nicolaus, M., 2014. Seasonal cycle and long-term trend of solar energy fluxes through Arctic sea ice, The Cryosphere, 8, 2219-2233, https://doi.org/10.5194/tc-8-2219-2014.

Comiso, J. C., 2012. Large decadal decline of the Arctic multiyear ice cover. J. Clim. 25, 1176–1193.

Corlett, W. B., Pickart, R. S., 2017. The Chukchi slope current. Prog. Oceanogr. 153, 50-65. doi:10.1016/j.pocean.2017.04.005

Dee, D. P., Uppala, S. M., Simmons, A. J., Berrisford, P., Poli, P., Kobayashi, S., Andrae, U., Balmaseda, M. A., Balsamo, G., Bauer, P., Bechtold, P., Beljaars, A. C. M., van de Berg, L., Bidlot, J., Bormann, N., Delsol, C., Dragani, R., Fuentes, M., Geer, A. J., Haimberger, L., Healy, S. B., Hersbach, H., Holm, E. V., ´ Isaksen, L., Ka llberg, P., Kohler, M., Matricardi, M., McNally, ¨ A. P., Monge-Sanz, B. M., Morcrette, J. J., Park, B. K., Peubey, C., de Rosnay, P., Tavolato, C., Thepaut, J. N., and Vitart, F., 2011. The ERA-Interim reanalysis: configuration and performance of the data assimilation system, Q. J. Roy. Meteor. Soc., 137, 553– 597.

Fukamachi, Y., Simizu, D., Ohshima, K., Eicken, H., Mahoney, A., Iwamoto, K., Moriya E., Nihashi, S., 2017. Sea-ice thickness in the coastal northeastern Chukchi Sea from moored ice-profiling sonar. Journal of Glaciology, *63*(241), 888-898. doi:10.1017/jog.2017.56

Gong, D., Pickart, R. S., 2015. Summertime circulation in the eastern Chukchi Sea. Deep-Sea Research II 118, 18–31.

Holland, M. M., Bitz, C. M., 2003. Polar amplification of climate change in coupled models, Clim. Dynam., 21, 221–232.

Itoh, M., Nishino, S., Kawaguchi, Y., Kikuchi, T., 2013. Barrow Canyon volume, heat, and freshwater fluxes revealed by long-term mooring observations between 2000 and 2008, J. Geophys. Res. Oceans, 118, 4363–4379, doi:10.1002/jgrc.20290.

Jackson, J. M., Carmack, E. C., McLaughlin, F. A., Allen, S. E., Ingram R. G., 2010. Identification, characterization, and change of the near-surface temperature maximum in the Canada Basin, 1993–2008, J. Geophys. Res., 115, C05021, doi:10.1029/2009JC005265.

Kalnay, E., Kanamitsu, M., Kistler, R., Collins, W., Deaven, D., Gandin, L., Iredell, M., Saha, S., White, G., Woollen, J., Zhu, Y., Leetmaa, A., Reynolds, B., Chelliah, M., Ebisuzaki, W., Higgins, W., Janowiak, J., Mo, K., Ropelewski, C., Wang, J., Jenne, R., Joseph, D., 1996. The NCEP/NCAR 40-Year Reanalysis Project. Bull. Amer. Meteor. Soc., 77, 437-471.

Lindsay, R., Wensnahan, M., Schweiger, A., Zhang, J., 2014. Evaluation of seven different atmospheric reanalysis products in the Arctic, J. Climate, https://doi.org/10.1175/JCLI-D-13-00014.1

Pegau, W. S., Paulson, C. A., 2001. The albedo of Arctic leads in summer, Annals of Glaciology, 33, 221-224.

Peng, G., Meier, W. N., Scott, D. J., Savoie, M. H., 2013. A long-term and reproducible passive microwave sea ice concentration data record for climate studies and monitoring, Earth Syst. Sci. Data, 5, 311-318, https://doi.org/10.5194/essd-5-311-2013

Perovich, D. K., Light, B., Eicken, H., Jones, K. F., Runciman, K., Nghiem, S. V., 2007. Increasing solar heating of the Arctic Ocean and adjacent seas, 1979–2005: attribution and role in the ice-albedo feedback, Geophys. Res. Lett., 34, L19505, doi:10.1029/2007GL031480.

Post, E., Bhatt, U. S., Bitz, C. M., Brodie, J. F., Fulton, T. L., Hebblewhite, M., Kerby, J., Kutz, S. L., Stirling, I., Walker, D. A., 2013. Ecological consequences of sea ice decline, Science, 341, 519–524, doi:10.1126/science.1235225.

Saha, S., Moorthi, S., Pan, H.-L., Wu, X., Wang, J., Nadiga, S., Tripp, P., Kistler, R., Woollen, J., Behringer, D., Liu, H., Stokes, D., Grumbine, R., Gayno, G., Wang, J., Hou, Y.-T., Chuang, H.- Y., Juang, H.-M. H., Sela, J., Iredell, M., Treadon, R., Kleist, D., Van Delst, P.,

Keyser, D., Derber, J., Ek, M., Meng, J., Wei, H., Yang, R., Lord, S., Van Den Dool, H., Kumar, A., Wang, W., Long, C., Chelliah, M., Xue, Y., Huang, B., Schemm, J.-K., Ebisuzaki, W., Lin, R., Xie, P., Chen, M., Zhou, S., Higgins, W., Zou, C.-Z., Liu, Q., Chen, Y., Han, Y., Cucurull, L., Reynolds, R. W., Rutledge, G., and Goldberg, M., 2010. The NCEP climate forecast system reanalysis, B. Am. Meteorol. Soc., 91, 1015–1057, doi:10.1175/2010BAMS3001.1.

Serreze, M. C., Barrett, A. P., Stroeve, J. C., Kindig, D. M., Holland, M., 2009. The emergence of surface-based Arctic amplification, Cryosphere, 3, 9–11.

Shimada, K., Kamoshida, T., Itoh, M., Nishino, S., Carmack, E., McLaughlin, F., Zimmermann, S., Proshutinsky, A., 2006. Pacific Ocean inflow: Influence on catastrophic reduction of sea ice cover in the Arctic Ocean, Geophys. Res. Lett., 33, L08605, doi:10.1029/2005GL025624.

Steele, M., Morison, J., Ermold, W., Rigor, I., Ortmeyer, M., Shimada, K., 2004. Circulation of summer Pacific halocline water in the Arctic Ocean, J. Geophys. Res., 109, C02027, doi:10.1029/2003JC002009.

Steele, M., Ermold, W., Zhang, J., 2008. Arctic Ocean surface warming trends over the past 100 years, Geophys. Res. Lett., 35, L02614, doi:10.1029/ 2007GL031651.

Steele, M., and Dickinson S., 2016. The phenology of Arctic Ocean surface warming, J. Geophys. Res. Oceans, 121, 6847–6861, doi:10.1002/ 2016JC012089.

Watanabe, E., 2011. Beaufort shelf break eddies and shelf-basin exchange of Pacific summer water in the western Arctic Ocean detected by satellite and modeling analyses, J. Geophys. Res., 116, C08034, doi:10.1029/2010JC006259.

Watanabe, E., Onodera, J., Itoh., M., Nishino, S., Kikuchi, T., 2017. Winter transport of subsurface warm water toward the Arctic Chukchi Borderland, Deep Sea Research Part I, 128, 115–130, doi:10.1016/j.dsr.2017.08.009.

Weingartner, T. J., Cavalieri, D. J., Aagaard, K., Sasaki, Y., 1998. Circulation, dense water formation, and outflow on the northeast Chukchi shelf. J. Geophys. Res., 103, 7647–7661.

Weingartner, T., Aagaard, K., Woodgate, R., Danielson, S., Sasaki, Y., Cavalieri, D., 2005. Circulation on the north central Chukchi Sea shelf. Deep-Sea Res. II. 52(24–26), 3150–3174. doi:10.1016/j.dsr2.2005.10.015.

Woodgate, R. A., Aagaard, K., Weingartner, T. J., 2006. Interannual changes in the Bering Strait fluxes of volume, heat and freshwater between 1991 and 2004, Geophys. Res. Lett., 33, 15609, doi:10.1029/2006GL026931.

Woodgate, R. A., Weingartner, T., Lindsay, R., 2010. The 2007 Bering Strait oceanic heat flux and anomalous Arctic sea-ice retreat, Geophys. Res. Lett., 37, 01602, doi:10.1029/2009GL041621.

Woodgate, R. A., Weingartner, T. J., Lindsay, R., 2012. Observed increases in Bering Strait oceanic fluxes from the Pacific to the Arctic from 2001 to 2011 and their impacts on the Arctic Ocean water column, Geophys. Res. Lett., 39, L24603, doi:10.1029/2012GL054092.

Woodgate, R.A., Stafford, K.M., Prahl, F.G., 2015. A synthesis of year-round interdisciplinary mooring measurements in the Bering Strait (1990–2014) and the RUSALCA years (2004–2011). Oceanography 28(3):46–67.

Table. 1 Correlation coefficients and standard deviations of absolute value of difference (W m^{-2}) between *in-situ* downward shortwave radiation obtained by the R/V Mirai and that from reanalysis products.

	NCEP-CFSR	ERA Interim	NCEP-NCAR Reanalysis 1
Correlation coefficient	0.81*	0.81*	0.75*
Standard deviation of absolute value of difference	10.81	18.02	18.71

* Significant at the 99% confidence level.

Figure captions

Fig. 1 Bottom topography (m) of the Chukchi Sea. The area enclosed by the solid black line indicates the area analyzed in this study (65.45°–75°N, 155°–180°W excluding the area where water depth > 200 m). Red dots indicate the locations of *in-situ* downward shortwave radiation observations by R/V Mirai (in 1999, 2002, 2004, 2006, 2008, 2009, and 2010) averaged over 24 hours.

Fig. 2 (a) Seasonal variation in sea-ice concentration averaged over the Chukchi Sea during 1999–2015 (black solid line) with ± 1 standard deviation from interannual variability (blue bars). (b) Seasonal variation in northward heat transport through the Bering Strait (TW) averaged during 1999–2015 (black solid line) with ± 1 standard deviation (red bars)

Fig. 3 Day-to-day variation of *in-situ* downward shortwave radiation obtained by R/V Mirai (black lines W m^{-2}) and downward shortwave radiation from NCEP-CFSR (red lines), ERA-Interim (purple lines) and NCEP/NCAR Reanalysis 1 (blue lines) (W m^{-2}) in (a) 1999, (b) 2002, (c) 2004, (d) 2006, (e) 2008, (f) 2009 and (g) 2010.

Fig. 4 Scatterplot of *in-situ* downward shortwave radiation obtained by R/V Mirai (W m^{-2}) and downward shortwave radiation from (a) NCEP-CFSR, (b) ERA-Interim and (c) NCEP/NCAR Reanalysis 1 (W m^{-2}).

Fig. 5 Horizontal distribution of cumulative solar heating from May to September in the Chukchi Sea averaged over 1999–2015 (10^8 Jm^{-2}) estimated using NCEP-CFSR downward shortwave radiation data.

Fig. 6 (a) Interannual variation in solar heating (red), total heating (black), sea-ice melting heat (blue), and the sum of the sensible heat (SH), latent heat (LH) and longwave radiation (LW) fluxes (green) integrated in the Chukchi Sea from May to September (10^{20} J). Purple line indicates northward heat flux through the Bering Strait (BSHF) integrated from May to September. (b) Interannual variation in downward shortwave radiation (red line, W m^{-2}) and the sea-ice concentration (blue line) averaged in the Chukchi Sea during May–September. (c) Interannual variation in northward heat flux through Barrow Canyon integrated from May to September (10^{20} J).

Fig. 7 Horizontal distribution of the correlation coefficient between the interannual variations in solar heating in each grid integrated from May to September and northward heat flux through Barrow Canyon integrated from May to September. Correlation coefficients of 0.5 and 0.75 mostly correspond to 90% and 99% confidence levels, respectively.

The English in this document has been checked by at least two professional editors, both native speakers of English. For a certificate, please see:
http://www.textcheck.com/certificate/Xni0ez

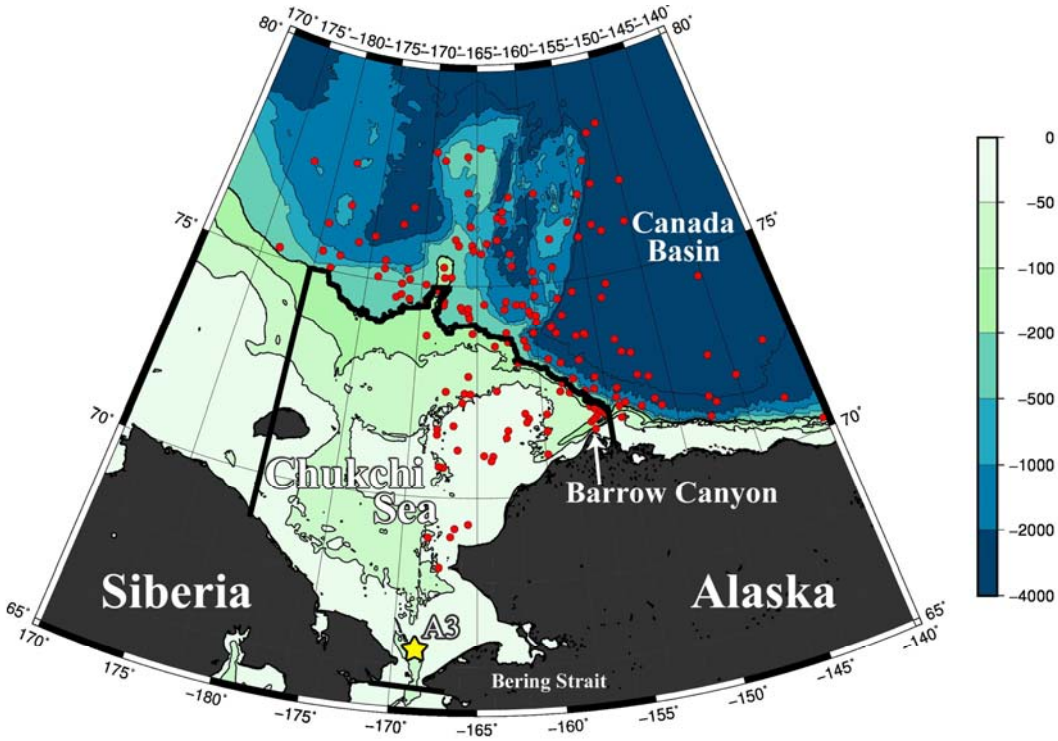

Fig. 1 Bottom topography (m) of the Chukchi Sea. The area enclosed by the solid black line indicates the area analyzed in this study (65.45°–75°N, 155°–180°W excluding the area where water depth > 200 m). Red dots indicate the locations of *in-situ* downward shortwave radiation observations by R/V Mirai (in 1999, 2002, 2004, 2006, 2008, 2009, and 2010) averaged over 24 hours.

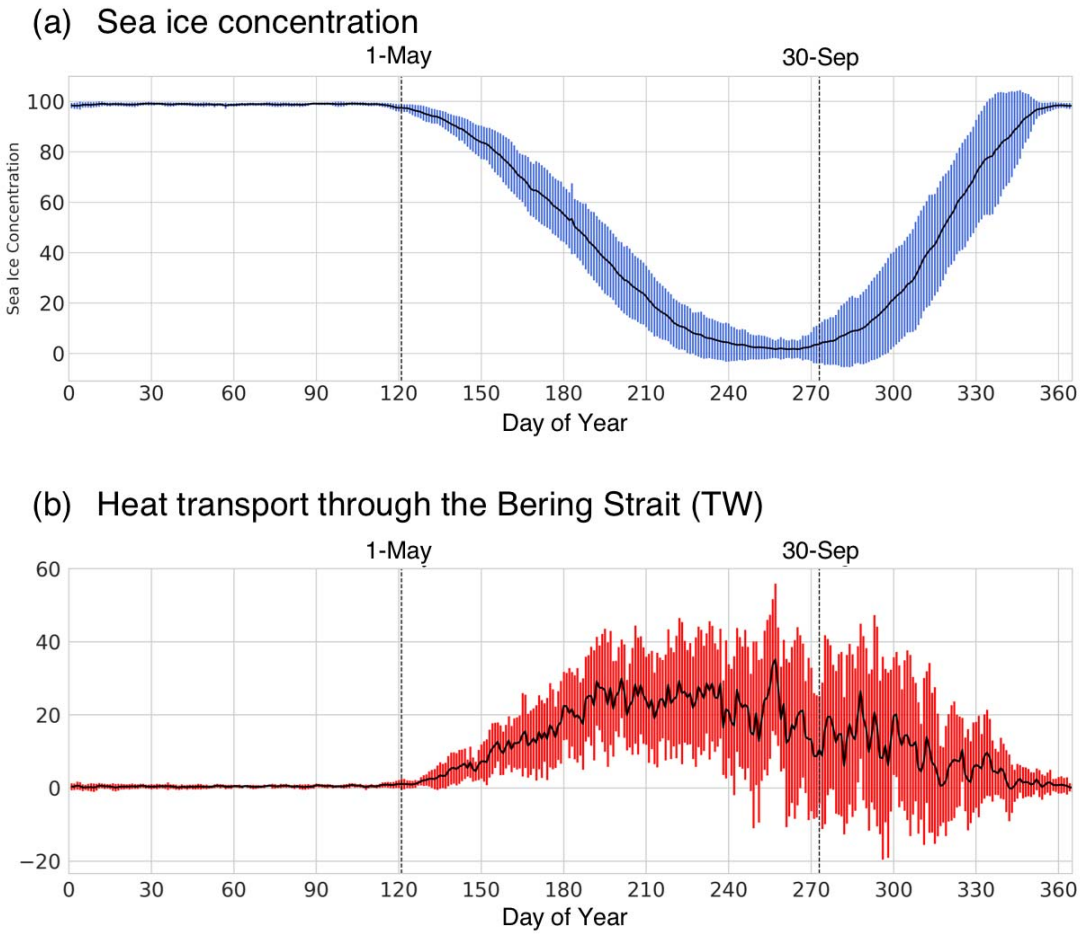

Fig. 2 (a) Seasonal variation in sea-ice concentration averaged over the Chukchi Sea during 1999–2015 (black solid line) with ± 1 standard deviation from interannual variability (blue bars). (b) Seasonal variation in northward heat transport through the Bering Strait (TW) averaged during 1999–2015 (black solid line) with ± 1 standard deviation (red bars)

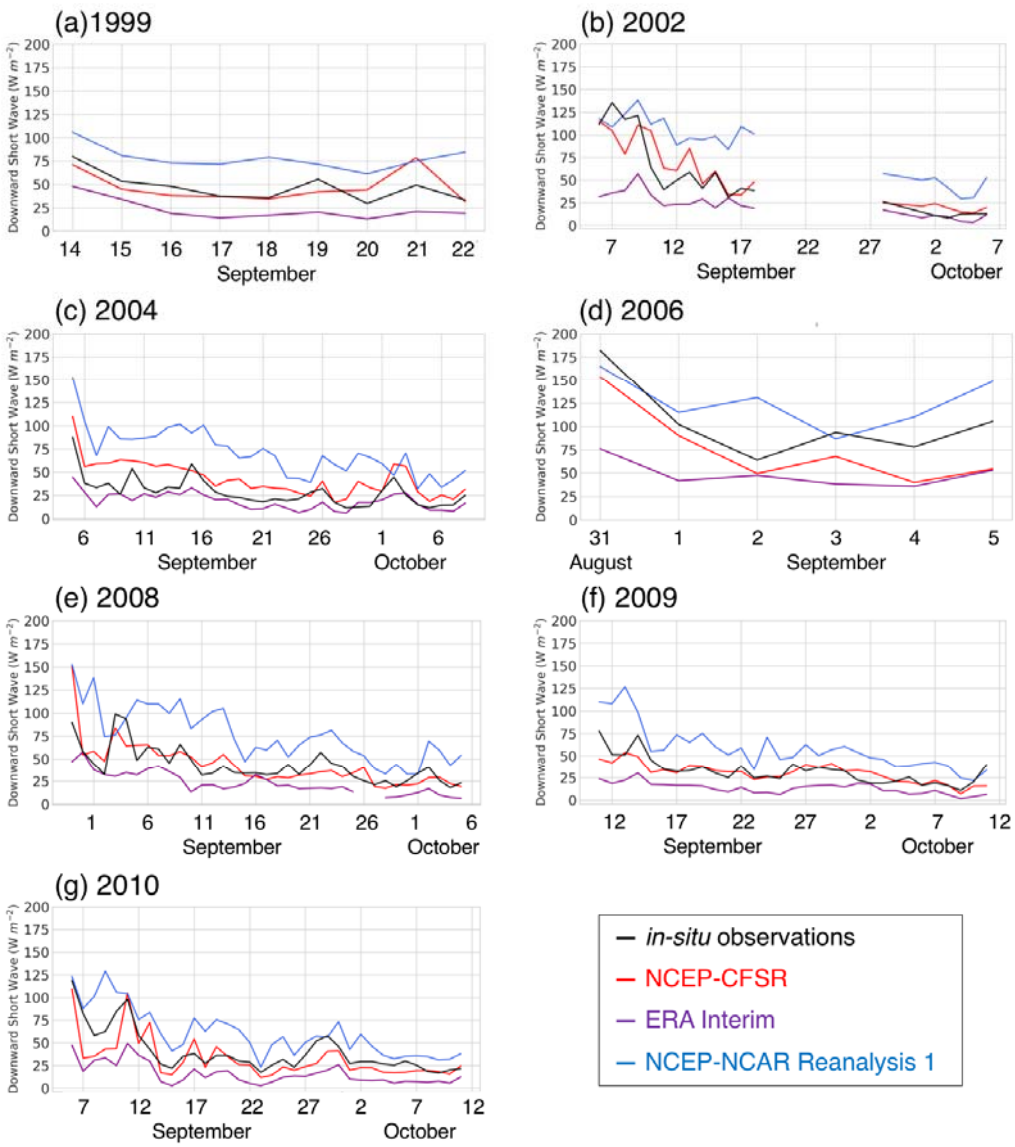

Fig. 3 Day-to-day variation of *in-situ* downward shortwave radiation obtained by R/V Mirai (black lines W m^{-2}) and downward shortwave radiation from NCEP-CFSR (red lines), ERA-Interim (purple lines) and NCEP/NCAR Reanalysis 1 (blue lines) (W m^{-2}) in (a) 1999, (b) 2002, (c) 2004, (d) 2006, (e) 2008, (f) 2009 and (g) 2010.

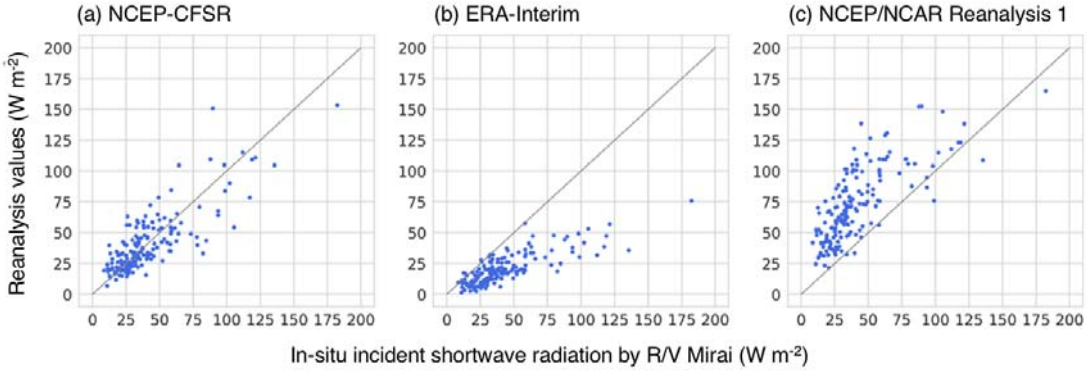

Fig. 4 Scatterplot of *in-situ* downward shortwave radiation obtained by R/V Mirai (W m^{-2}) and downward shortwave radiation from (a) NCEP-CFSR, (b) ERA-Interim and (c) NCEP/NCAR Reanalysis 1 (W m^{-2}).

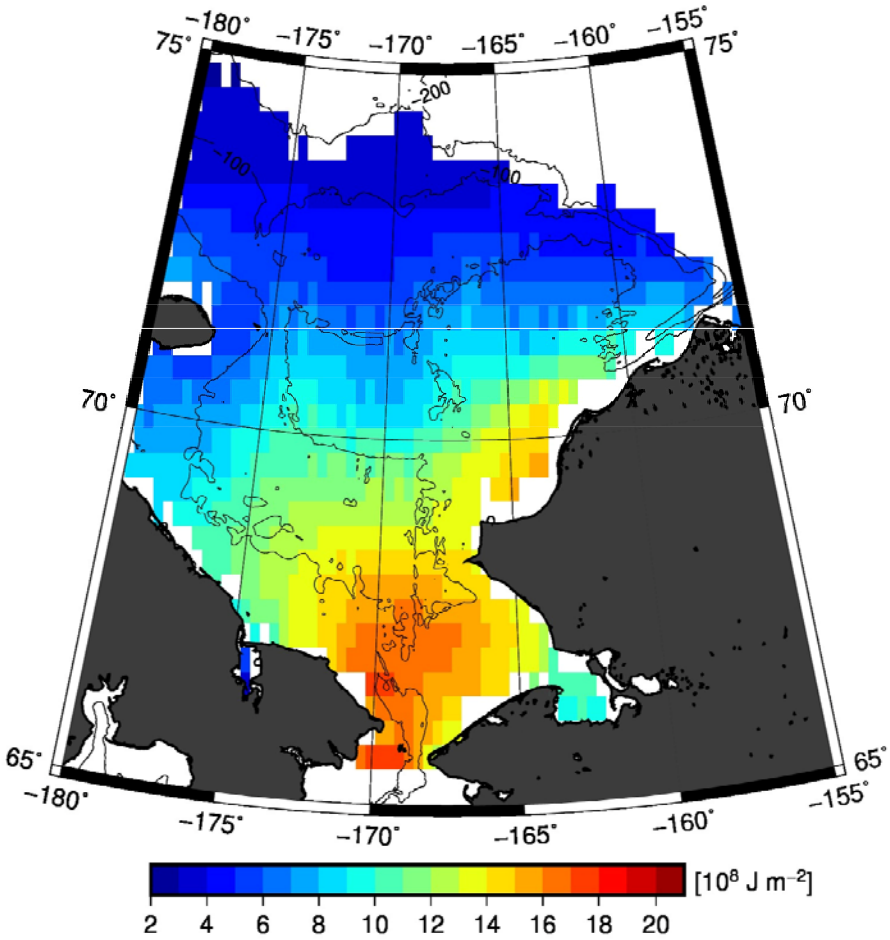

Fig. 5 Horizontal distribution of cumulative solar heating from May to September in the Chukchi Sea averaged over 1999–2015 (10^8 Jm^{-2}) estimated using NCEP-CFSR downward shortwave radiation data.

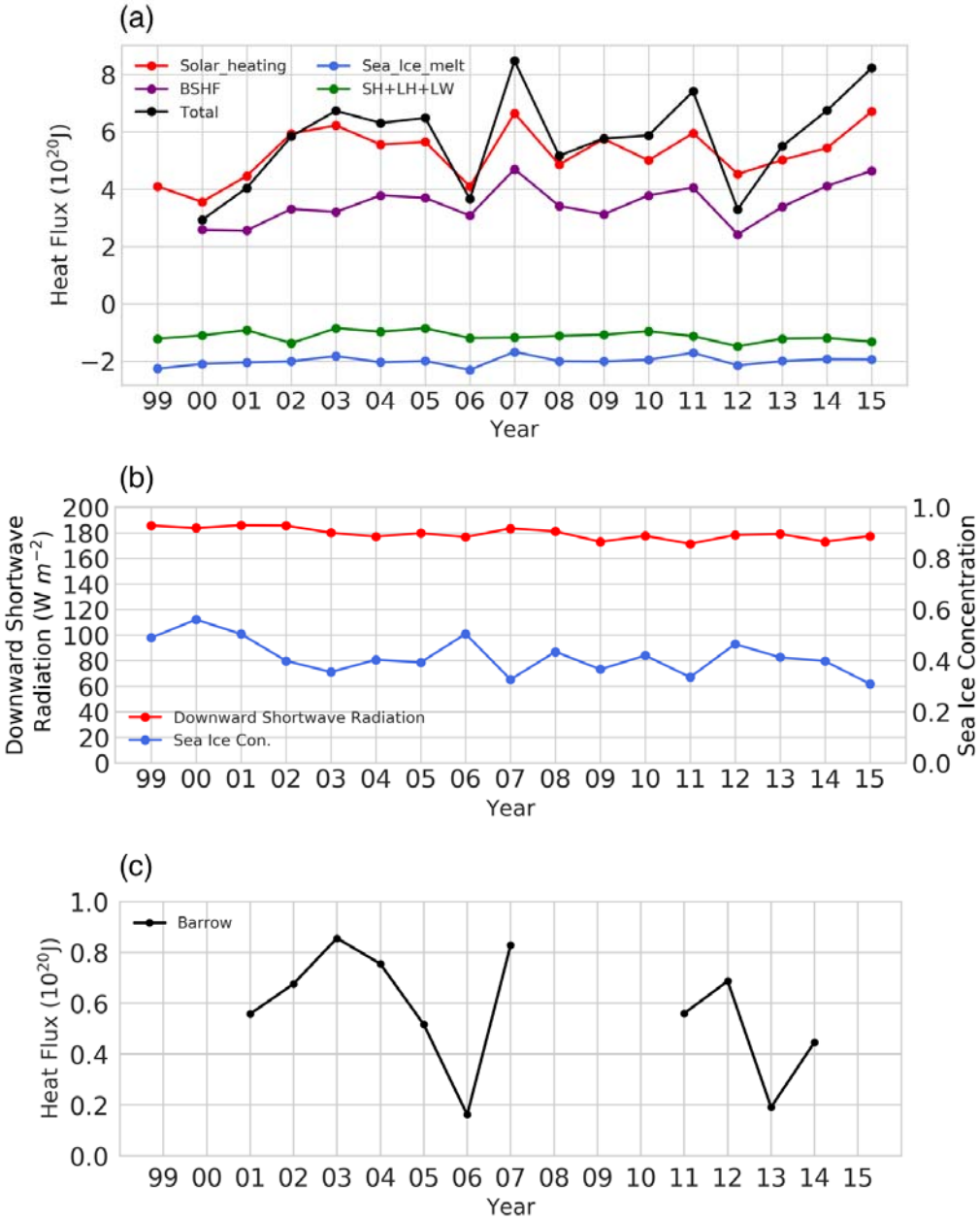

Fig. 6 (a) Interannual variation in solar heating (red), total heating (black), sea-ice melting heat (blue), and the sum of the sensible heat (SH), latent heat (LH) and longwave radiation (LW) fluxes (green) integrated in the Chukchi Sea from May to September (10^{20} J). Purple line indicates northward heat flux through the Bering Strait (BSHF) integrated from May to September. (b) Interannual variation in downward shortwave radiation (red line, W m^{-2}) and the sea-ice concentration (blue line) averaged in the Chukchi Sea during May–September. (c) Interannual variation in northward heat flux through Barrow Canyon integrated from May to September (10^{20} J).

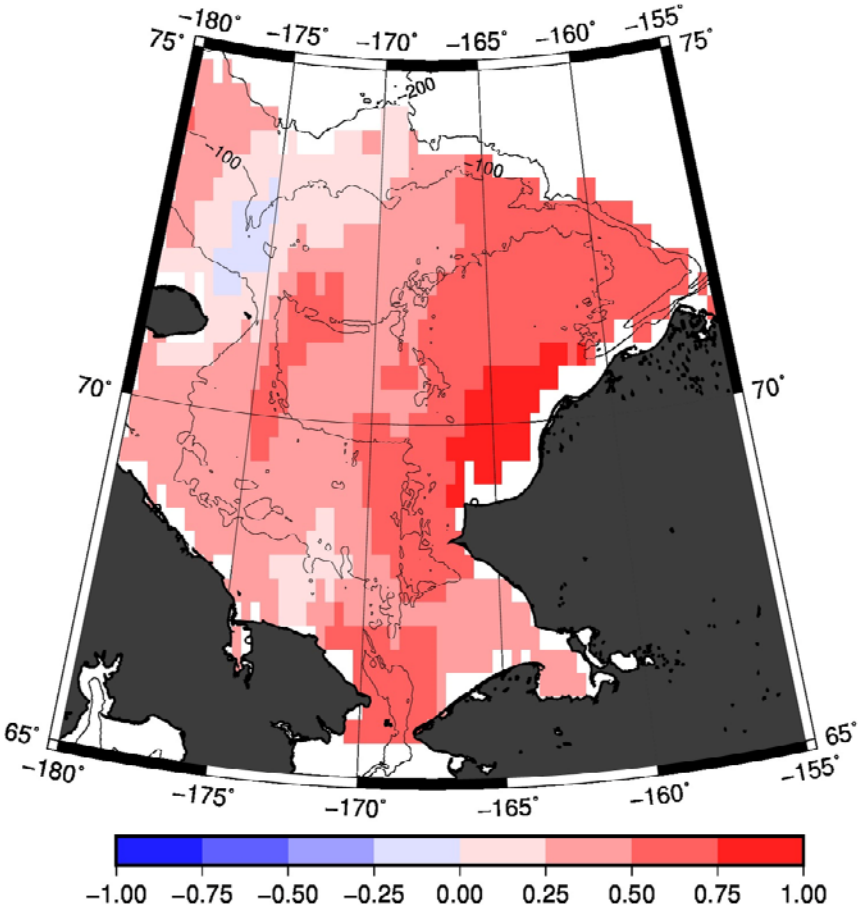

Fig. 7 Horizontal distribution of the correlation coefficient between the interannual variations in solar heating in each grid integrated from May to September and northward heat flux through Barrow Canyon integrated from May to September. Correlation coefficients of 0.5 and 0.75 mostly correspond to 90% and 99% confidence levels, respectively.